Enhancement in nanoscale electrical properties of lead zirconic titanate island fabricated by focused ion beam

R.H. Liang, Denis Remiens, D. Deresmes, Caroline Soyer, David Troadec, X.L. Dong, L.H. Yang, R. Desfeux, A. da Costa, J.F. Blach

Enhancement in nanoscale electrical properties of lead zirconic titanate island fabricated by focused ion beam

Cite as: J. Appl. Phys. **105**, 044101 (2009); https://doi.org/10.1063/1.3073892
Submitted: 25 May 2008 • Accepted: 12 December 2008 • Published Online: 17 February 2009

R. H. Liang, D. Rémiens, D. Deresmes, et al.

Enhancement in nanoscale electrical properties of lead zirconic titanate island fabricated by focused ion beam

R. H. Liang,[1,a)] D. Rémiens,[1] D. Deresmes,[1] C. Soyer,[1] D. Troadec,[1] X. L. Dong,[2] L. H. Yang,[2] R. Desfeux,[3] A. Da Costa,[3] and J. F. Blach[3]
[1]*Institut of Electronique, Microélectronique and Nanotechnology (IEMN), CNRS-UMR 8520, Cité scientifique, Villeneuve d'Ascq 59655, France*
[2]*Shanghai Institute of Ceramics, Chinese Academy of Sciences, 1295 Dingxi Road, Shanghai 200050, People's Republic of China*
[3]*Unité de Catalyse et de Chimie du Solide (UCCS), CNRS-UMR 8181, Faculté des Sciences Jean Perrin, Université d'Artois, Rue Jean Souvraz, SP 18, Lens Cedex 62307, France*

(Received 25 May 2008; accepted 12 December 2008; published online 17 February 2009)

Lead zirconic titanate (PZT) microscale island (1 μm–100 nm) was fabricated by focused ion beam before its crystallization, followed by the annealing treatment at the crystallization temperature. Local electrical properties were evaluated by piezoresponse force microscopy technique. Compared to the PZT island fabricated after crystallization, the result shows that there is noticeable enhancement in nanoscale electrical properties of PZT island fabricated before crystallization, especially when the island size decreases. Raman spectra and Kelvin force microscopy result both show that there are little degradations on the PZT surface after this amorphous etching process. The mechanism will be discussed in this paper. These results are very beneficial to the development of the ferroelectric film applications in the dynamic random access memory, ferroelectric random access memory, and micro-electro-mechanical system field. © *2009 American Institute of Physics*. [DOI: 10.1063/1.3073892]

I. INTRODUCTION

In the past decade, ferroelectric films have received a worldwide technological interest for a large number of applications such as optoelectronic, memory devices [dynamic random access memory (DRAM), ferroelectric random access memory (FERAM)], and micro-electro-mechanical systems (MEMSs).[1–3] Among the various ferroelectric films, $Pb(Zr_x,Ti_{1-x})O_3$ film is one of the most used materials because of its large remnant polarization (P_r), small coercive field (E_c), and large piezoelectric coefficient (d_{33}). In view of the practical applications point, one of the main process objectives in the integration of lead zirconic titanate (PZT) ferroelectric capacitors into memory devices or MEMS applications is developing the ability to pattern these ferroelectric films and associated electrode materials by etching. Several techniques have been developed: wet chemical etching,[4] ion beam etching (IBE),[5] reactive ion etching,[6] electrocyclotron resonance etching,[7] and inductively coupled plasma etching.[8] Despite the large amount of effort in this field, there are still some problems that need to be overcome. One of the main challenges is to develop the etching process with no degradation in the electrical properties of the film or device. Generally speaking, the remnant polarization (P_r) decreases, coercive field (E_c) increases, and the internal field appears after etching process, and these are attributed to the physical defects induced by the ion bombardment, the chemical contamination of surface absorbed residue, and stress-induced effects. The etching damage is more severe when the pattern size of PZT film is decreased to nanometer dimensions because of the "sidewall effect." Recently, much attention has been paid to minimize the etching damage. According to Torii *et al.*,[9] the leakage current density in micron-size capacitors is increased several times compared to in larger ones due to increased contributions from the damaged region of the capacitor sidewalls. So some researchers attempted post-annealing treatment in O_2 gas after etching to reduce the etching damage; however the electrical properties cannot be completely recovered by O_2 annealing.[10] Lee *et al.*[11] improved the electrical properties using a wet cleaning method, but this method may change the etch profile of the film and the lateral dimension of the pattern. Song *et al.*[12] investigated several etching mask technologies to choose proper mask for etching and found that TiO_2/PSG/TiN and PSG/TiN masks (PSG for phosphore silicate glass) were effective in minimizing the etching damage. Typically, PZT thin film is etched after its crystallization. Some authors have also published results concerning the characterization of PZT films of nanoscale size.[13–15] In this study, the submicrometer PZT island (1 μm–100 nm) is patterned on amorphous film by focused ion beam (FIB) method and then annealed at its crystallization temperature. With these etching and annealing conditions, there is a great enhancement in nanoscale electrical properties of PZT islands and the mechanism will also be discussed in the text.

II. EXPERIMENTAL

$LaNiO_3$ has been verified to be a favorable bottom electrode for ferroelectric film capacitor applications because its lattice parameter can match well with the ferroelectric film and the oxide electrodes can also act as a sink for oxygen vacancies and prevent their accumulation at the film/

[a)]Author to whom correspondence should be addressed. Tel.: 0086-21-69987780. Electronic mail: liangruihong@mail.sic.ac.cn.

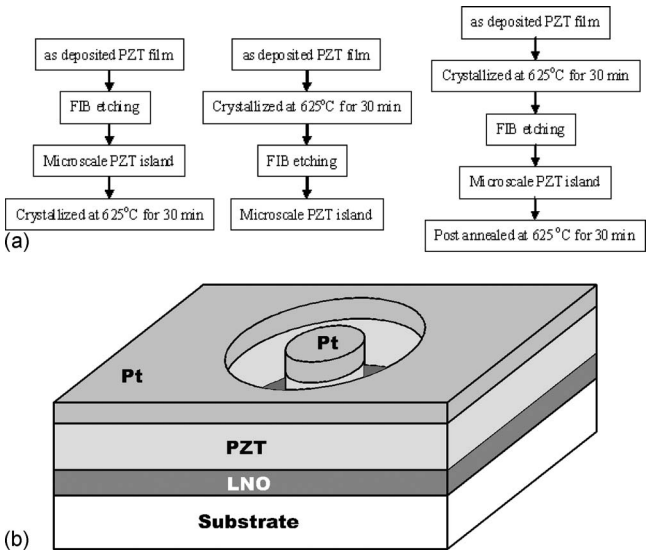

FIG. 1. Flow chart of (a) amorphous FIB etching process, (b) conventional FIB etching process, (c) conventional FIB etching process after postannealing at 625 °C, and (d) schematic of FIB fabrication of PZT island structure.

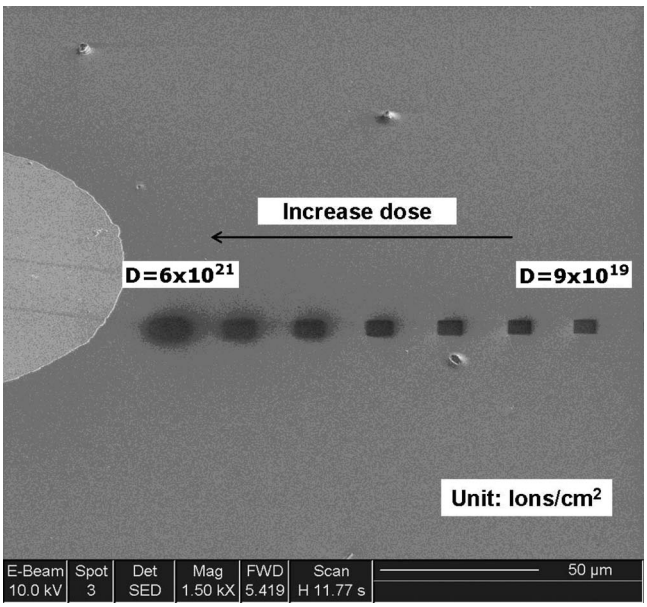

FIG. 2. FIB exposed PZT layer with different Ga ion doses.

electrode interface. Moreover, based on the previous research of our group, ferroelectric films deposited on the $LaNiO_3$ coated SiO_2/Si substrate with (100) preferred orientation have better piezoelectric properties compared to films on Pt coated substrate.[16] So, in this work, a $LaNiO_3$ film with thickness of 250 nm, deposited by rf magnetron sputtering, was chosen as the bottom electrode. $PbZr_{0.53}Ti_{0.47}$ film with thickness of 300 nm was deposited on the $LaNiO_3$ coated SiO_2/Si substrate by rf magnetron sputtering with no postannealing. Then this amorphous PZT film was patterned by FIB to fabricate the PZT microscale island ($1\ \mu m - 100$ nm). FIB patterning here was performed in FEI Dual Beam STRATA 235 with a Ga^{+3} ion beam, an acceleration voltage of 30 kV, and a beam current of 300 pA (corresponding to 25 nm spot size) at normal incident angle. Before etching, a thin 100–120 nm Pt top electrode was deposited on the PZT film surface by dc sputtering. It can protect the PZT island from etching damage and has also served as top electrode. Then these amorphous PZT microscale islands were annealed at the crystallization temperature of 625 °C for 30 min. In this paper, for simplicity, this etching process is called amorphous etching. For comparison, microscale PZT islands with same thickness and size were also fabricated by the conventional FIB etching process, which means etching on the annealed crystallized PZT samples. The postannealing effect after conventional etching is also investigated. In three cases their local electrical properties were examined. Figures 1(a)–1(c) are the flow charts of the three different etching processes and (d) is the schematic view of the FIB fabrication of PZT island structure.

For investigating the electrical properties of PZT islands, local piezoelectric hysteresis loops produced by a commercial atomic force microscope (AFM) (Multimode, Nanoscope IIIa, Digital Instruments) were recorded for the measurement of the coercive voltage V_c, phase switch, and amplitude of the relative piezoelectric-response signal. The experiments are carried out by considering the so-called "in-field" mode, which presents the particular characteristic, to be very close to the one used for "macroscopic" hysteresis loops recording.[17–19] In brief, in this mode, a continuous bias voltage is applied between the tip and the ground bottom electrode together with an alternative voltage of the form $V = V_{ac}\cos(2\pi ft)$ which can induce the vibration of the sample. The signal generated by the piezoelectric vibration (PFM) and feedback from the photodetector to a lock-in amplifier is of the form $A\cos\phi$. The amplitude A of the first harmonic signal of the vibration is related to the piezoelectric coefficients of the sample, while the phase shift ϕ between the alternative reference voltage and the first harmonic signal depends on the direction of the polarization in the film. For our experiments, platinum/iridium coated silicon tips with a stiffness of 40 N/m were used. The dc voltage was gradually changed from -10 to $+10$ V within a period of 1 s. The voltage step was adjusted to 0.4 V. The frequency of the ac voltage was 2 kHz with a 1.5 V driving voltage.

To simulate and analyze the FIB induced damage in the PZT island sidewall layer, another FIB etching experiment was performed, as shown in Fig. 2. Additional large squares ($7\times 7\ \mu m$) were FIB exposed at the surface of PZT film using different ion doses to investigate sidewall damage. The ion dose is controlled by the etching time. The lightest exposal is performed with an ion dose of about 9×10^{19} ions/cm^2 participating and the hardest is done with 6×10^{21} ions/cm^2 participating. Accordingly the FIB exposed area was separately fabricated by two different etching processes: one is amorphous etched and the other is conventional etched. Raman spectra in the $200-1000$ cm^{-1} range were carried out with a Dilor XY-800 confocal micro-Raman spectrometer. The Raman spectra were recorded using the 514.5 nm line of an Ar/Kr ion laser. The incident laser beam was focused on the FIB exposed area with 1 μm spot size and 10 mW power. The surface potential of the FIB exposed PZT surface by different etching process was performed by Kelvin force microscopy (KFM) technique. KFM experi-

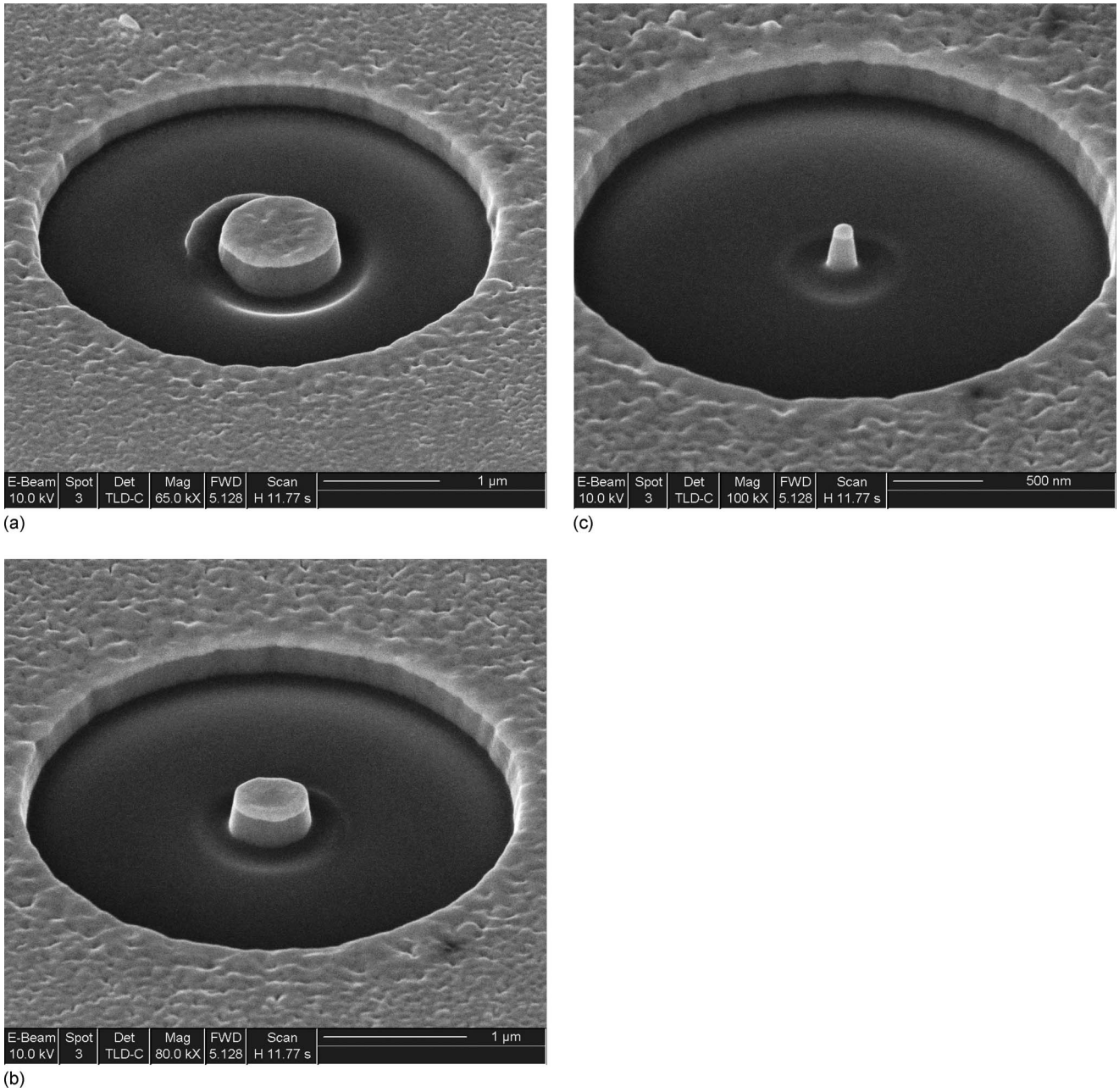

FIG. 3. The morphology of PZT island with different diameters: (a) 1 μm, (b) 500 nm, and (c) 100 nm.

ments here were carried out on a Dimension 3100 microscope (Veeco Digital Instruments). The platinum coated tip was used with the frequency of 70–80 kHz and the spring constant of 1–5 N/m.

III. RESULTS AND DISCUSSIONS

The morphologies of PZT islands with different sizes are shown in Fig. 3. Because the profile of the island is almost the same for different etching processes, only one group of island is shown here.

Figures 4–6 separately show the typical phase (a) and amplitude (b) of first harmonic signal of 1 μm, 500 nm, and 100 nm PZT islands fabricated by different etching processes. From these figures, it can be clearly seen that the PZT island fabricated by amorphous FIB etching process has much better electrical properties compared to conventional FIB etching, especially when the island size decreases. For 1 μm PZT island, the average coercive voltage $[Va=(Vc^+ - Vc^-)/2]$ of PZT island fabricated by amorphous FIB etching (0.5 V) is much lower than the one fabricated by conventional etching process (2.7 V). This means the domain switching of PZT island becomes more difficult after conventional etching process. Additionally, large internal voltage $(V_i=Vc^+ + Vc^-)$ appears after conventional FIB etching and the value is about 2.5 V. The amplitude of first harmonic signal of PZT island by amorphous FIB etching is nearly 2.5 times larger than the one by conventional FIB etching. The postannealing effect after conventional etching is also investigated. With up to 625■ postannealing in atmosphere for 30 min, the average coercive voltage decreases but still 1 V higher; the amplitude increases but still lower than the

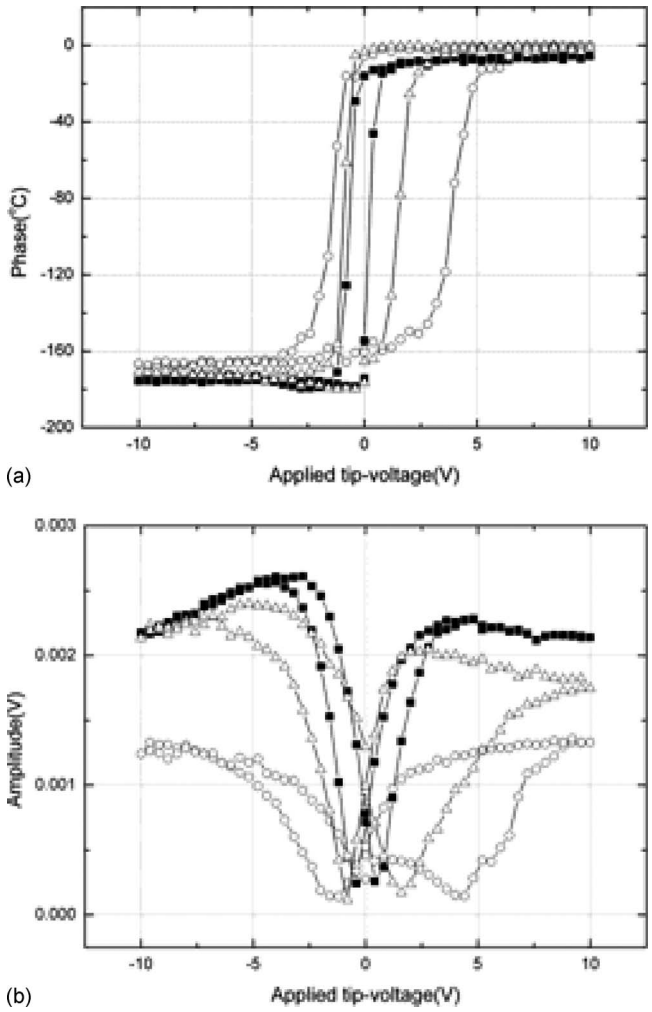

FIG. 4. (a) Typical phase and (b) amplitude of first harmonic signal of 1 μm PZT island fabricated by ■ amorphous FIB etching process, ○ conventional etching process, and □ after postannealing at 625 °C.

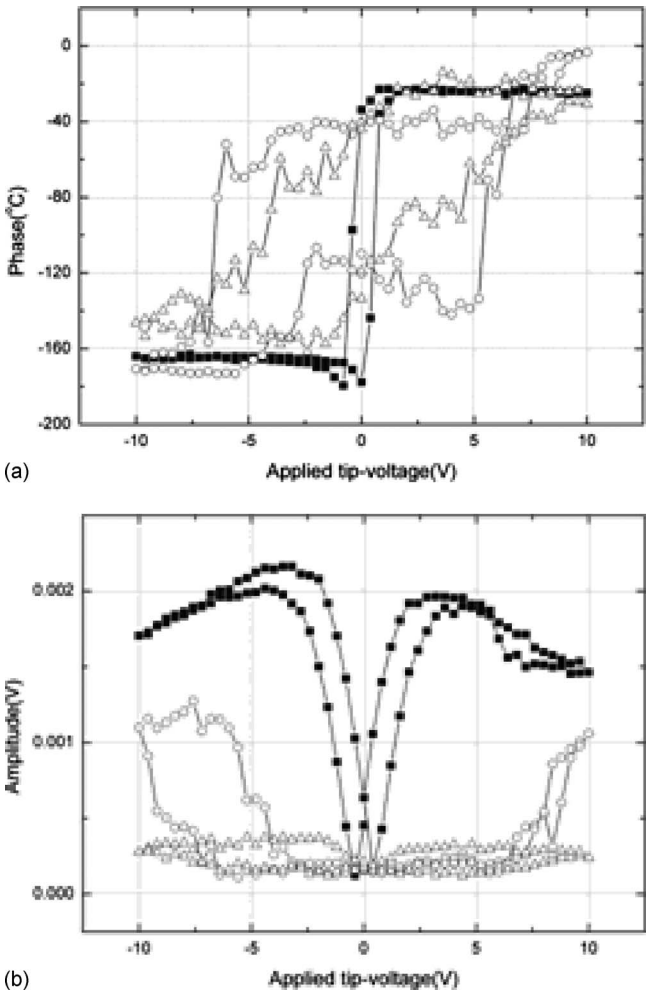

FIG. 5. (a) Typical phase and (b) amplitude of first harmonic signal of 500 nm PZT island fabricated by ■ amorphous FIB etching process, ○ conventional etching process, and □ after postannealing at 625 °C.

sample fabricated by amorphous FIB etching process. It implies that the atmosphere postannealing can compensate for the defects induced by the conventional etching process but can only partially recover the electrical properties. When the island size decreases to 500 nm, the degradation of electrical properties after conventional etching is more serious, which is shown in Fig. 5, while the electrical properties of 500 nm PZT island fabricated by amorphous FIB etching are almost unchanged. Also there is neither domain switching nor piezoelectric amplitude in 100 nm PZT island fabricated by conventional etching process, even after the postannealing treatment. This notable degradation of electrical properties of PZT island fabricated by conventional FIB etching may be attributed to the sidewall effect, which is more serious when the PZT island size decreases. So, we can get the conclusion that there is great a enhancement in the nanoscale electrical properties on PZT island fabricated by amorphous FIB etching process. Based on the equation piezoresponse (a.u.)$=A \times \cos \phi$, the relative piezoresponse of PZT island fabricated by amorphous etching with different size is shown in Fig. 7. When the size of the PZT island decreases especially to 100 nm, the piezoresponse signal increases notably, which could be due to the decrease in the substrate clamping effect. Another explanation could be induced by the existence of parasitic effect due to "in air" electrostatic interaction between the AFM tip and the film surface. This effect increases when the PZT island diameter decreases.[20] In Fig. 6(a), the hysteresis loop of 100 nm PZT island is slim and the coercive voltage is smaller compared to 1 μm or 500 nm PZT island, which means the domain switching is easier, and it is also in part probably due to the decrease in the substrate clamping effect.

From the above results of local electrical properties of PZT islands, it can be seen that if FIB etching is performed before PZT crystallization, the nanoscale electrical properties of PZT islands can be greatly improved compared to conventional etching process, especially when the island size decreases. We attribute this phenomenon to the possibility that the sidewall damage can be diluted if the PZT island is fabricated by amorphous FIB etching process. To confirm this assumption additional large squares (7×7 μm) were FIB exposed at the surface of PZT film using different ion doses to investigate sidewall damage and the details of the experiment are mentioned above. Raman and KFM experiments were performed on these patterns. Figure 8 shows the Raman spectra of (a) unexposed crystallized PZT film, (b) after

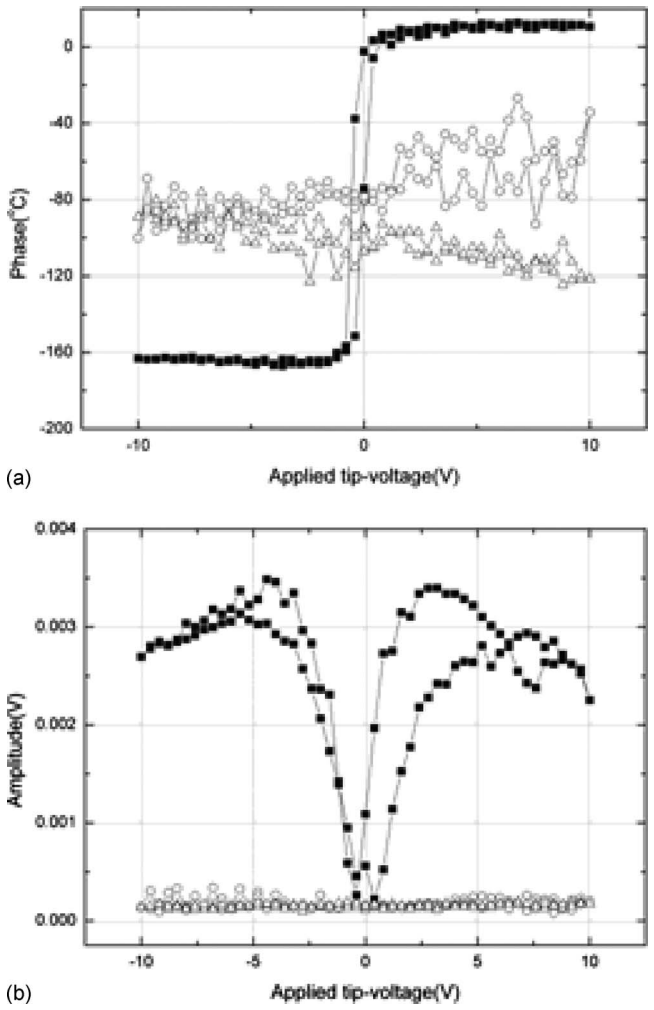

FIG. 6. (a) Typical phase and (b) amplitude of first harmonic signal of 100 nm PZT island fabricated by ■ amorphous FIB etching process, ○ conventional etching process, and □ after postannealing at 625 °C.

hardest amorphous FIB etching (6×10^{21} ions/cm^2 dose participating), (c) after lightest (9×10^{19} ions/cm^2), and (d) hardest conventional FIB etching (6×10^{21} ions/cm^2). In the spectra, the broadband centered at 280, 572, and 676 cm^{-1}

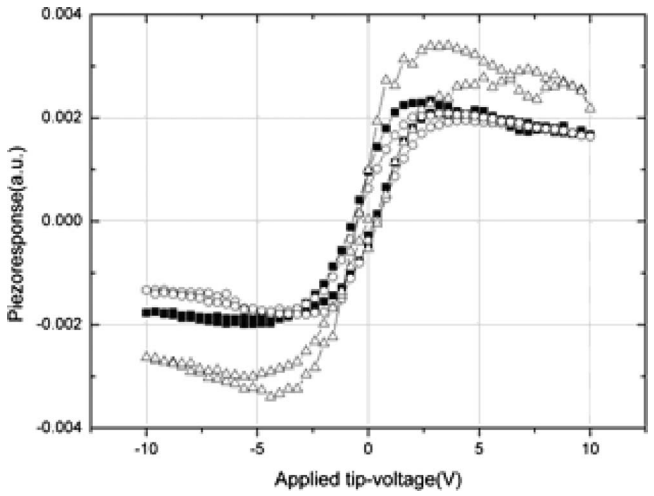

FIG. 7. Relative piezoresponse of PZT island fabricated by amorphous etching with different sizes: ■ 1 μm, ○ 500 nm, and □ 100 nm.

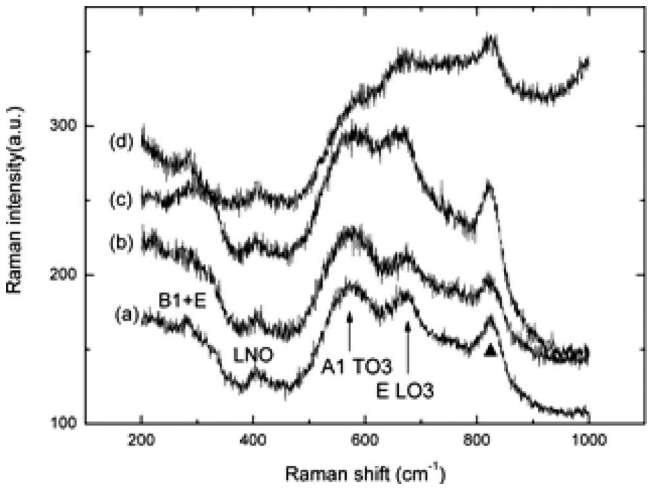

FIG. 8. Raman spectra of (a) unexposed crystallized PZT film (b) after hardest amorphous FIB etching (6×10^{21} ions/cm^2 dose participating), (c) after lightest (9×10^{19} ions/cm^2), and (d) hardest conventional FIB etching (6×10^{21} ions/cm^2)

can be assigned as B_1+E, $A_1(TO_3)$, and $E(LO_3)$ according to the modes in the single PZT crystals.[21] The band centered at 820 cm^{-1} is tentatively assigned to Ti–O bond.[22] The band detected at 400 cm^{-1} is attributed to LNO. After the hardest amorphous etching process, the spectra profile of PZT surface is almost unchanged compared to the unetched PZT film surface. For the region after the lightest conventional FIB etching, the spectrum has not almost changed, except that the intensity of the Raman peak at 676 cm^{-1} increases, while for the hardest conventional etching case, Raman spectra recorded in the region exposed to the FIB show noticeable change. The sharp increase in the intensity of the Raman band at 676 cm^{-1} [$E(LO_3)$ mode] may be connected with the distortion of the tetragonal symmetry of the PZT crystalline lattice due to the ion implantation and the modification of the stress state.[23–25] The broadening of Raman scattering in 550–900 cm^{-1} region may be attributed to the existence of the amorphous material, which is usually expected during the conventional FIB etching process. Whatever the FIB etching process is, the peak position of Raman shift does not show any change, which means that the crystalline structure still exhibits perovskite phase.

Figure 9 presents the KFM image of the region after the hardest amorphous FIB etching (a) and hardest conventional etching process (b). KFM experiments were made on the two samples with the same tip during the same day, so the experimental error can be almost ignored. It shows that the surface potential is changed after etching, especially for the region exposed to conventional FIB. To see it more clearly, the absolute surface potential value across the etching region is shown in Fig. 10. It implies that the potential difference between the unetched surface and the surface after amorphous etching is very small (only about 15 mV), while the difference between the unetched surface and the surface after conventional FIB etching is very large (about 300 mV). This result indicates that the surface after conventional FIB etching is dramatically changed and damaged, while the surface exposed to amorphous FIB etching is almost unchanged, which is corresponding to the above Raman result.

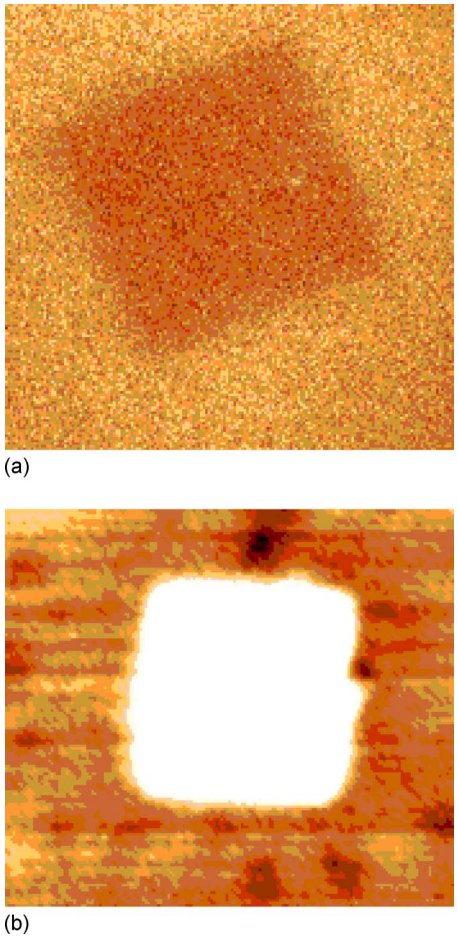

FIG. 9. (Color online) KFM image of the region (a) after hardest amorphous FIB etching and (b) hardest conventional etching process.

From the Raman spectra and KFM result, it can be clearly seen that amorphous FIB etching can reduce the etching damage on the surface. We attribute this to three following reasons. One is that this method can reduce the surface roughness induced by etching. In our previous paper, the grain boundary is favorably etched because there is excess lead at the grain boundary and the lead oxide etching rate is higher than titanium or zirconium oxide.[26] Moreover, lateral etching that induces the grain boundary widening can add to the etching process. Excess physical atom bombardment can occur at the grain boundary, which results in the quick etching rate at this local area, and then increases the roughness after etching. On the other hand, the etching rate is anisotropic on the crystalline structure. The effect of Ga ion bombardment is different, which depends on the atom density. Different crystal plane orientation has different atom density, so the etching rate is different and the roughness increases after etching. If the FIB etching is performed before PZT crystallization, there is neither grain boundary nor crystalline structure, so the etching rate can be almost regarded as isotropic and the roughness will be reduced. For our experiment the roughness of the region after amorphous FIB etching is 1.2 nm, while the roughness of the region after conventional FIB etching is about 5 nm. Roughness reduction can improve the electrical properties of PZT film. The second reason is that for amorphous etching process, the damaged layer on amorphous PZT film surface induced by Ga ion bombardment can be almost crystallized into the ferroelectric perovskite phase by the following annealing treatment and there is little degradation on the surface, which is shown in the above Raman and KFM result. Charge defects on the PZT surface after etching may also be reduced after following the annealing treatment and this will avoid the possibility of "short circuit" on the sidewall. During the island etching, the Ga ion implantation is just on the sidewall of the island but after annealing, Ga ions can migrate into the crystal lattice of PZT island and there are fewer charge defects left on the sidewall. The third reason is that there is no domain in the amorphous PZT film, and it is well known that the charge defects induced by the ion bombardment can limit the domain mobility and increase the coercive voltage, which can be proved by the results in Figs. 4–6. This effect will not exist in amorphous FIB etching case. Roughness reduction, little degradation in the surface, and no domain etching can effectively reduce the sidewall effect and make the amorphous FIB etching process a very promising etching way with no degradation in electrical properties, especially when the island size decreases. To confirm the effectiveness of the amorphous etching method, the IBE process was also conducted on the amorphous PZT film, followed by the annealing step at the perovskite crystallization temperature. No damaged layer can be observed on the surface of the etched PZT film by this amorphous etching process. Compared to the unetched PZT film, there is no or very little degradation in the dielectric, ferroelectric, and piezoelectric properties. The details can be found in our last paper and will not be shown here.[27] This further confirms that amorphous etching process can reduce the etching damage and this is very beneficial to the development of the ferroelectric film application in the field of DRAM, FERAM, and MEMS applications.

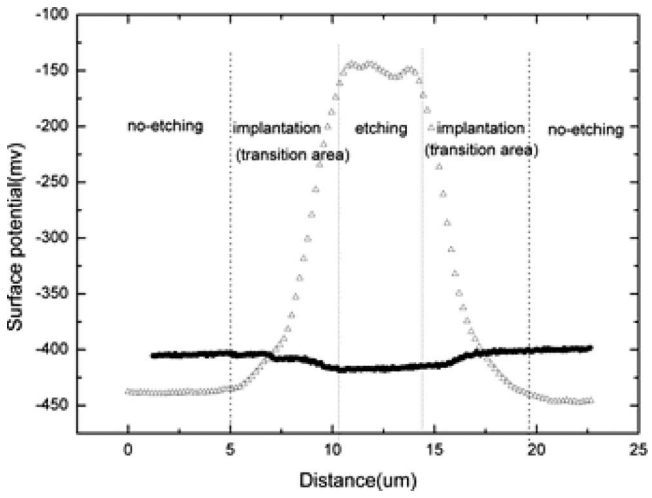

FIG. 10. Absolute surface potential value across the region ■ after hardest amorphous FIB etching and □ hardest conventional etching process.

ACKNOWLEDGMENTS

This work was supported by the postdoctoral project provided by the France ministry of research and new technology. The authors also want to thank the Université de Valenciennes et du Hainaut Cambrésis.

[1]J. F. Scott and C. A. P. de Araujo, Science **246**, 1400 (1989).
[2]M. Moallem, M. R. Kermani, R. V. Patel, and M. Ostojic, IEEE Trans. Control Syst. Technol. **2**, 757 (2004).
[3]A. M. Flyn, L. S. Tavrow, S. F. Bart, R. A. Brooks, D. J. Ehrlich, K. R. Udayakumar, and L. E. Cross, J. Microelectromech. Syst. **1**, 44 (1992).
[4]S. Mancha, Ferroelectrics **135**, 131 (1992).
[5]T. Kawagughi, H. Adachi, K. Setsune, O. Yamazaki, and K. Wasa, Appl. Opt. **23**, 2187 (1984).
[6]K. Saito, J. H. Choi, T. Fukuda, and M. Ohue, Jpn. J. Appl. Phys., Part 2 **31**, L1260 (1992).
[7]S. Yokoyama, Y. Ito, K. Ishihara, K. Hamada, T. Ohnishi, J. Kudo, and K. Sakiyama, Jpn. J. Appl. Phys., Part 1 **34**, 767 (1995).
[8]C. W. Chung and C. J. Kim, Jpn. J. Appl. Phys., Part 1 **36**, 2747 (1997).
[9]K. Torii, H. Kawakami, H. Miki, K. Kushida, T. Itiga, Y. Goto, T. Kumihashi, N. Yokoyama, M. Moniwa, K. Shoji, T. Kaga, and Y. Fujisaki, Integr. Ferroelectr. **16**, 21 (1997).
[10]M. G. Kang, K. T. Kim, and C. I. Kim, Thin Solid Films **435**, 222 (2003).
[11]J. K. Lee, T. Y. Kim, I. Chung, and S. B. Desu, Appl. Phys. Lett. **75**, 334 (1999).
[12]Y. J. Song, N. W. Jang, S. Y. Lee, D. J. Jung, H. H. Kim, S. H. Joo, J. K. Lee, and K. Kim, Integr. Ferroelectr. **37**, 47 (2001).
[13]C. S. Ganpule, A. Stanishevsky, Q. Su, S. Aggarwal, J. Melngailis, E. Williams, and R. Ramesh, Appl. Phys. Lett. **75**, 409 (1999).
[14]M. Alexe, C. Harnagea, D. Hesse, and U. Gösele, Appl. Phys. Lett. **75**, 1793 (1999).
[15]C. S. Ganpule, A. Stanishevsky, S. Aggarwal, J. Melngailis, E. Williams, and R. Ramesh, Appl. Phys. Lett. **75**, 3874 (1999).
[16]M. Detalle, G. Wang, D. Rémiens, P. Ruterana, P. Roussel, and B. Dkhil, J. Cryst. Growth **305**, 137 (2007).
[17]R. Desfeux, C. Legrand, A. Da Costa, D. Chateigner, R. Bouregba, and G. Poullain, Surf. Sci. **600**, 219 (2006).
[18]C. Legrand, A. Da Costa, R. Desfeux, C. Soyer, and D. Rémiens, Appl. Surf. Sci. **253**, 4942 (2007).
[19]A. Ferri, A. Da Costa, R. Desfeux, M. Detalle, G. S. Wang, and D. Rémiens, Integr. Ferroelectr. **91**, 80 (2007).
[20]S. Tiedke *et al.*, Appl. Phys. Lett. **79**, 3678 (2001).
[21]J. F. Meng, R. S. Katiyar, and G. T. Zou, Phys. Status Solidi A **164**, 851 (1997).
[22]X. Lou, X. Hu, M. Zhang, F. D. Morrison, S. A. T. Redfern, and J. F. Scott, J. Appl. Phys. **99**, 044101 (2006).
[23]J. Frantti, V. Lantto, S. Nishio, and M. Kakihana, Phys. Rev. B **59**, 12 (1999).
[24]J. F. Meng, R. S. Katiyar, G. T. Zou, and X. H. Wang, Phys. Status Solidi A **164**, 851 (1997).
[25]K. Nomura, Y. Takeda, M. Maeda, and N. Shibata, Jpn. J. Appl. Phys., Part 1 **39**, 5247 (2000).
[26]C. Soyer, E. Cattan, and D. Rémiens, J. Appl. Phys. **92**, 1048 (2002).
[27]R. H. Liang, D. Rémiens, C. Soyer, N. Sama, X. L. Dong, and G. S. Wang, Microelectron. Eng. **85**, 670 (2008).